A Different Outflow Length Scale?

DORON NOF* AND STEPHEN VAN GORDER

Department of Oceanography, The Florida State University, Tallahassee, Florida

THIERRY PICHEVIN

EPSHOM/CMO, Brest, France

(Manuscript received 18 February 2003, in final form 11 September 2003)

ABSTRACT

Using a nonlinear ''reduced gravity'' model it is shown analytically that a large buoyant midlatitude outflow situated along the northern boundary of a β-plane ocean produces an unusually broad westward flow. The steady nonlinear outflow consists of a narrow jet (whose width is the familiar midlatitude Rossby radius) and a broad, nearly stagnant region whose width is the *equatorial* Rossby radius. The steady, inviscid solution reported here is constructed with the aid of the momentum-flux equation. For high-Rossby-number flows (i.e., zero potential vorticity flows), the total outflow's width is $\sim$1.228 times the equatorial Rossby radius. A finite potential vorticity outflow produces a slightly narrower westward flow. The above solution breaks down in the linear limit, and it is expected that a linear outflow would consist of a single flow whose width is on the order of the midlatitude Rossby radius. Numerical simulations are in very good agreement with the above nonlinear solution. The new southward outflow solution reported here complements recently derived solutions for *northward* outflows, *eastward* outflows, and *westward* outflows. In the earlier northward outflow case (i.e., a light water source situated along a southern boundary), a chain of westward-propagating eddies and an eastward current are produced. This corresponds to the situation in the Gulf of Mexico where Loop Current eddies are generated. In the earlier eastward outflow case (i.e., a light water source situated along a western boundary), a steady gyre is generated. This corresponds to the Tsugaru gyre (in the western Pacific) and the Alboran gyre (in the western Mediterranean). In the earlier westward outflow case (i.e., a source situated along an eastern boundary), a chain of westward-propagating eddies and a *northward* current are produced. (The Southern Hemisphere analog of this case corresponds to the generation of teddies and the Leeuwin Current.) A new solution with the new length scale corresponds to outflows such as the one associated with the surface flow (from the Atlantic to the Caribbean) through the Windward or Mona Passage. At present, there are no observations that can support or reject the scales suggested by the authors.

1. Introduction

The manner in which water of anomalous density empties (from a point source) into an ocean has been of theoretical interest to oceanographers for decades. In everyday life, a source of anomalous water emptying into a large container tends to spread evenly in all directions. In the ocean, however, the earth's rotation tends to confine the outflow to the coast (in the Kelvin wave sense) forming an alongshore current. Various attempts have been made to understand how the anomalous water is distributed once it debouches into an f-plane ocean (e.g., Takano 1954, 1955; Defant 1961, chapter 16; Nof 1978a,b; Garvine 1987, 1996, 2001; Chao and Boicourt 1986; O'Donnell 1990; Oey and Mellor 1993; Kourafalou et al. 1996; Yankovsky and Chapman 1997). By and large, these studies assume that an outflow on an f plane ultimately reaches a steady state. They show a clear turning of the flow to the right and a gyre to the right of the exit. Recent analytical and numerical studies have shown that an inviscid outflow from a point source on an f plane cannot be steady (see Pichevin and Nof 1997; Nof and Pichevin 2001). Furthermore, numerical simulations and analytical work demonstrate that the outflow balloons in the sense that a forever-growing eddy is generated near the coast (Pichevin and Nof 1997; Fong 1998; Nof and Pichevin 2001; Horner et al. 2000); that is, a part of the outflow goes into a gyre and the remaining part goes into a boundary current.

These f-plane results are consistent with those of Whitehead (1985) who showed that a jet impinging on a wall must split into two branches. There are, of course,

* Additional affiliation: Geophysical Fluid Dynamics Institute, The Florida State University, Tallahassee, Florida.

Corresponding author address: Dr. Doron Nof, Dept. of Oceanography 4320, The Florida State University, Tallahassee, FL 32306-4320.
E-mail: nof@ocean.fsu.edu

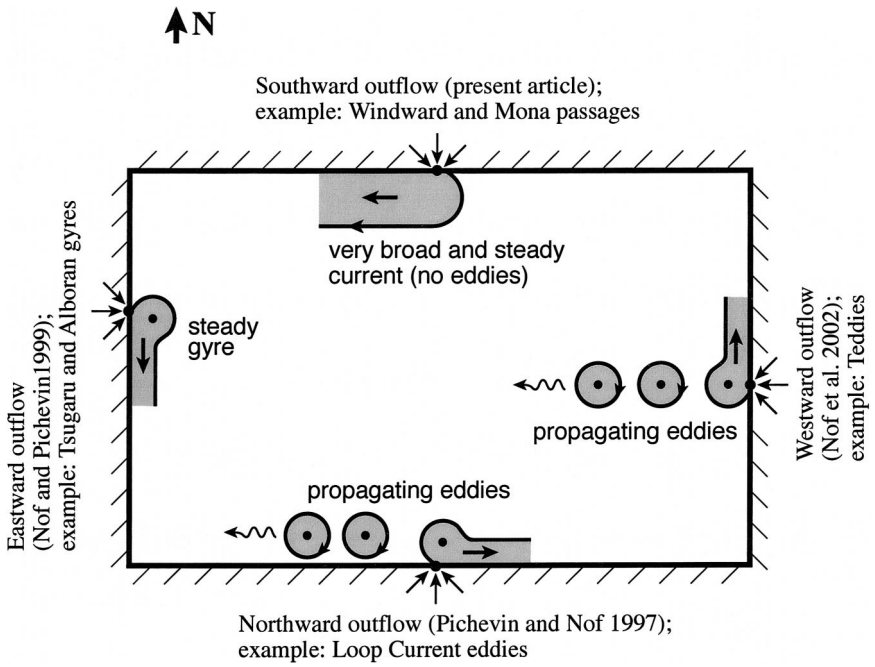

FIG. 1. The four scenarios of the β-plane outflow problem: a northward outflow (Pichevin and Nof 1997) is situated next to a southern boundary, a westward outflow is situated along an eastern boundary (Nof et al. 2002), a southward outflow is situated next to a northern boundary (present article), and an eastward outflow is situated next to a western boundary (Nof and Pichevin 1999). The southward outflow, which is the focus of this study, is the only case in which neither a steady gyre nor eddies are formed.

exceptions to the general nonsteady solution—an outflow from a channel oriented almost parallel to the coast can be steady (Garvine 2001; Horner et al. 2000) because the momentum-flux deficit is very small and an outflow from a gradually broadening channel can also be steady (Whitehead and Miller 1979; Bormans and Garrett 1989) because the excess momentum flux is exerted on the walls.

On a β plane (which is our focus here) the situation is still more complicated. There are four possible scenarios—a northward outflow, a westward outflow, a southward outflow, and an eastward outflow (Fig. 1)—all of which have different solutions. Of these four, three outflows (northward, westward, and eastward) involve eddies or gyres. These three have been addressed previously in Pichevin and Nof (1997), Nof and Pichevin (1999), and in Nof et al. (2002). The last unsolved case of this category, which is the focus of this study, is the southward outflow (which, as we shall see, does not involve eddies). Ironically, it is the simplest solution of the four and yet was the most difficult for us to obtain (probably because we erroneously assumed a priori that it would also involve eddies). We shall show analytically in sections 2 and 3 that the formation of a very broad current is a fundamental property of any nonlinear *southward outflow* regardless of the fluid's vorticity. It results from the impossibility of balancing the flow force (associated with the alongshore current) without the establishment of such a broad current.

Using a numerical reduced-gravity model (of the Bleck and Boudra type) we shall then show that, as the analytical solution predicts, the variation of the Coriolis parameter with latitude produces such a broad current (section 4). The derivation of this solution as well as the proceeding numerical simulations are the main new aspects of this article. Last, possible application of the models to the surface flow in the Windward and Mona Passages is discussed and the results are summarized (section 5).

2. Formulation

This section describes the physics of the problem and the mathematical approach. Consider a southward point source carrying relatively light water (of density ρ) emptying into an otherwise stagnant ocean (with density $\rho + \Delta\rho$). As the light current exits the point source it must turn to the right (in the Northern Hemisphere) and hug the coast because this is the direction in which Kelvin waves will propagate and this is the only place where such a current can have a finite cross-sectional area. As in Nof (1988), Pichevin and Nof (1997), and Nof and Pichevin (1999, 2001), we will neglect the point source contribution to the alongshore momentum flux.

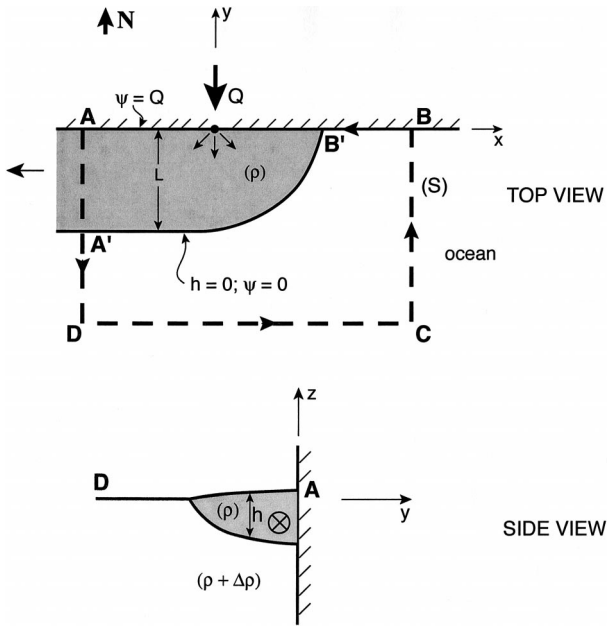

FIG. 2a. Schematic diagram of the model under study. A southward source carrying water with density (ρ) empties into an otherwise stagnant ocean with density ($\rho + \Delta\rho$). Assuming (and later verifying with the numerical simulations) that there is an inviscid steady state corresponding to the current hugging the coastline on the right-hand side (looking downstream), one finds that the momentum imparted on the region bounded by ADCBA by the water exiting through AD is balanced by the westward β force associated with the current. Without loss of generality we may choose $\psi = 0$ along the front ($h = 0$).

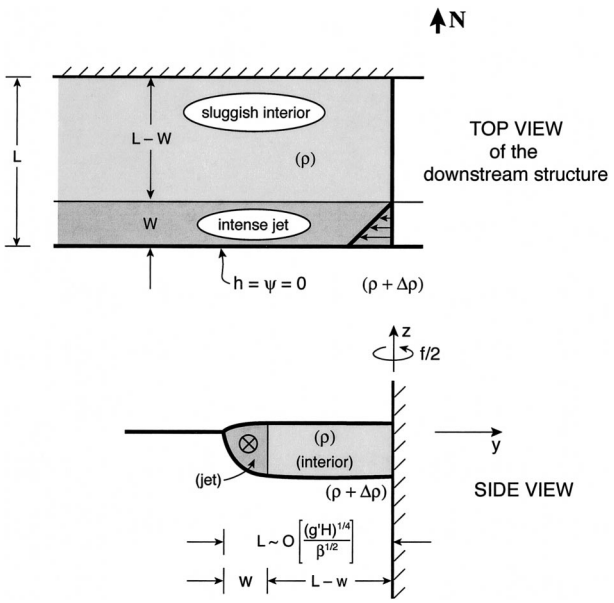

FIG. 2b. Schematic diagram of the downstream flow (i.e., the flow in section AD shown in Fig. 2a). Next to the wall a broad, nearly stagnant region is established. This region is of the *equatorial* Rossby radius scale. On the left-hand side (looking downstream) a swift jet (with the conventional midlatitude Rossby radius width) is established. In the zero potential vorticity case (shown), the velocity within the jet is linearly distributed and goes to zero along the edge of the stagnant region. In the finite potential vorticity case (not shown), the velocity decays exponentially to zero. The undisturbed thickness H is related to the outflow's mass flux Q by $H = (2f_0Q/g')^{1/2}$.

This is done on the grounds that, at the point source, the velocities go to infinity because of the finite mass flux and infinitesimal cross-sectional area. The local Rossby number (based on the velocities and dimensions of the point source) is, therefore, infinite implying that, at the point source and its immediate vicinity, the effect of the earth's rotation is negligible. Consequently, just like the familiar potential flow solution for a point source, our source is symmetrical relative to the y axis [i.e., u_s, the speed at the source, obeys $u_s(y) = u_s(-y)$] despite the presence of rotation [see, e.g., Nof (1988), his Fig. 4 and section 7]. Although it is not necessary, one can alternatively assume that the outflow is fed by a very narrow channel (perpendicular to the coast) containing streamlines parallel to the channel walls (see Pichevin and Nof 1997).

Assuming that, on a β plane, a steady state can be reached and integrating the steady nonlinear alongshore momentum equation over the (fixed) region (S) bounded by the dashed line ADCBA shown in Fig. 2a we get

$$\int\int_S \left(hu\frac{\partial u}{\partial x} + hv\frac{\partial u}{\partial y} - fvh + g'h\frac{\partial h}{\partial x} \right) dx\,dy = 0, \quad (2.1)$$

where $f = f_0 + \beta y$, h is the thickness of the light water (i.e., $h \equiv 0$ outside the current), S is the integration area, and the remaining notation is conventional. (Note that, for convenience, the variables are defined in both the text and the appendix.) We shall see shortly that (2.1) implies a balance between the β-induced excess Coriolis force resulting from the turning of the fluid (as it exits the source) and the momentum flux of the downstream jet. This balance is $\beta yvh \sim O(hu\,\partial u/\partial x)$. Using continuity, we find that this balance implies an outflow width L given by

$$L \sim (U/\beta)^{1/2} \sim (g'H)^{1/4}/\beta^{1/2},$$

which is the equatorial Rossby radius. This outflow scaling is identical to the Rhines eddy length scale (Rhines 1975) but the similarity between the two is simply due to the fact that the equatorial Rossby radius is a fundamental property, so it is relevant to many different problems. In contrast to the Rhines scale, our present scale is not derived from turbulent eddy dynamics and, more important, it involves inertial rather than geostrophic terms.

Using the continuity equation and a streamfunction ψ (defined by $\partial\psi/\partial x = vh$; $\partial\psi/\partial y = -uh$), (2.1) can be written as

$$\int\int_S \left[\frac{\partial}{\partial x}(hu^2) + \frac{\partial}{\partial y}(huv) \right] dx\,dy - \int\int_S f\frac{\partial\psi}{\partial x}\,dx\,dy + \frac{g'}{2}\int\int_S \frac{\partial(h^2)}{\partial x}\,dx\,dy = 0, \quad (2.1a)$$

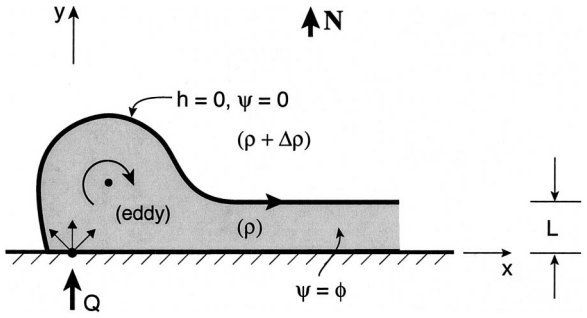

FIG. 3. A schematic diagram of the (hypothetical) steady configuration shown by Pichevin and Nof (1997) and Nof and Pichevin (2001) to be impossible on both an f plane and on a β plane. In this scenario, a steady inviscid outflow cannot exist because the alongshore momentum flux of the downstream current is not balanced. As a result of this impossibility, the eddy grows and the downstream current mass flux q is smaller than the incoming mass flux Q. On a β plane, the eddy detaches periodically from the source because, once it reaches a large enough size, its westward drift exceeds its growth rate.

which, with the aid of Green's theorem, can be simplified to

$$\oint_{\phi} huv\,dx - \oint_{\phi} (hu^2 + g'h^2/2 - f\psi)\,dy = 0, \quad (2.1b)$$

where ϕ is the boundary of S.

Noting that along the zonal boundary (i.e., $dy \equiv 0$) at least one of the three variables h, u, and v is zero and, defining $\psi = 0$ where $h = 0$, one finds that (2.1b) can also be written as

$$\int_{-L}^{0} (hu^2 + g'h^2/2 - f\psi)\,dy = 0. \quad (2.2)$$

Assuming (and later verifying with our numerical experiments) that the downstream flow (Fig. 2b) is parallel to the wall and, hence, geostrophic in CD (so that $fu = -g'\partial h/\partial y$, which, upon multiplication by h and integration in y from the current edge to a point within the current, gives $f\psi = g'h^2/2 + \beta\int_{-L}^{y} \psi\,dy$), relation (2.2) reduces to the simple relationship

$$\int_{-L}^{0} hu^2\,dy - \beta\left[\int_{-L}^{0}\left(\int_{-L}^{y} \psi\,dy\right)dy\right] = 0, \quad (2.3)$$

where L is the unknown width of the current downstream.

Equation (2.3) is the key to our solution. The first term is the simple well-known jet force, but the second is not so simple and is not so well known. Several comments should be made before discussing its meaning. First, (2.3) shows that, in the absence of β (i.e., an f-plane outflow), a nonlinear outflow can never have a steady solution because the jet force [i.e., the first term in (2.3)] cannot be balanced. This case was discussed in detail in Pichevin and Nof (1997) and Nof and Pichevin (2001) who showed that a forever-growing eddy

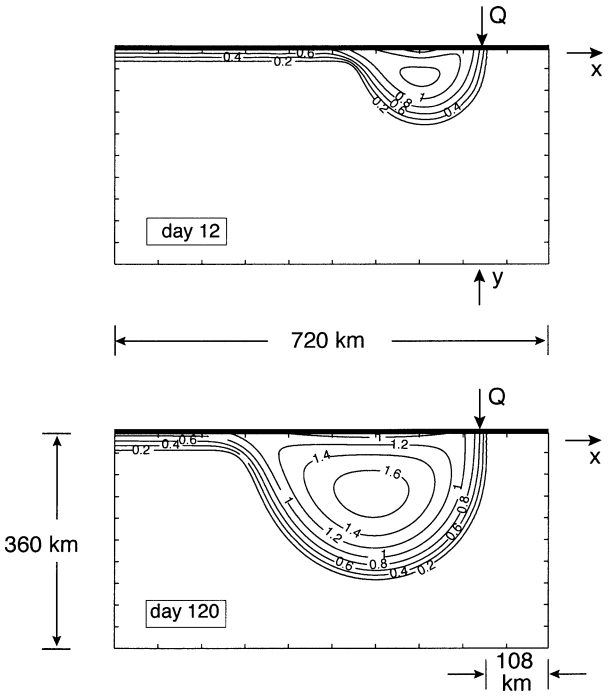

FIG. 4. Nondimensional f-plane thickness contours (h/H) for a zero PV outflow. Note that the gyre is growing in time. Physical constants: $f = 10^{-4}$ s^{-1}; $g' = 2 \times 10^{-2}$ m s^{-2}; $Q = 20$ Sv; $R_d = 30$ km; $H = 450$ m; grid size $\Delta x = \Delta y = 3.6$ km; time step, $\Delta t = 5$ min; eddy viscosity, 360 m^2 s^{-1}. Adapted from Nof and Pichevin (2001).

(bulge) is established near the mouth (Figs. 3 and 4). Namely, in this case, part of the mass flux goes into a steadily growing eddy and the remaining part goes into an alongshore current. Note that, in the linear limit, a steady f-plane outflow is possible because the velocity and its square are very small so that (2.3) is automatically satisfied.

Second, in the nonlinear limit considered here, a steady solution can be established only if the second term (the β force) balances the first (the jet force). Since $\beta R_d/f$ is usually small [$\sim O(0.01)$], we immediately see that, in order for this to happen, L must be large. It is a simple matter to see that, under such conditions, $L \sim O[(g'H)^{1/4}/\beta^{1/2}]$; that is, the flow scale must be of the *equatorial* Rossby radius, which is equivalent to stating that $L \sim O[R_d/(\beta R_d/f)^{1/2}]$. We shall see later that the manner in which the flow achieves this large width is as follows. Near the coast a broad nearly stagnant region (with the equatorial Rossby radius scale L) is generated. Adjacent to this sluggish region a jet of conventional Rossby radius is established (on the ocean side). Hence, the jet force that we speak about is analogous to that associated with a conventional boundary current. The β force, on the other hand, is primarily associated with the region near the source where the outflow turns toward the west. Physically, this means that the outflow simply broadens itself until it is wide enough for the two terms in (2.3) to balance each other. As mentioned,

it is not a simple matter to understand what the second represents and why it is a westward force. This is explained in the next section.

Third, the above balance of forces holds regardless of the fluid's potential vorticity (PV). The nearly stagnant region is established by friction that comes in and alters the potential vorticity until the necessary vorticity is created. Last, we point out that the above balance of forces may not exist in the case of a curved coastline or a bottom topography that depends on x because, under such conditions, the flow force may be exerted on the bottom rather than the fluid. We shall return to this important point in section 6.

We shall now explain the nature of the second (β) term in (2.3). The origin of the term is the planetary vorticity gradient force:

$$F_\beta = \int\int_S (f v h - g' h h_x)\, dx\, dy, \tag{2.4}$$

where, for the southward outflow case, S is the shaded area in Fig. 2a. We first note that the Bernoulli principle [$(u^2 + v^2)/2 + g'h = \text{const}$ along a streamline] implies that the velocity is constant along the front ($h = 0$). Next, we note that downstream (say, at A′ shown in Fig. 2a) the Coriolis force associated with this velocity is balanced by the pressure gradient force. Upstream, where the southward frontal flow turns westward (section B′A′ shown in Fig. 2a), there is a larger Coriolis parameter (due to β) implying a larger Coriolis force and an excess westward force. This is why (2.4) implies a *westward* force.

In our present situation (southward outflow), the flow reaches a steady state simply by expanding to a length scale comparable to the equatorial Rossby radius. In the northward outflow case discussed by Pichevin and Nof (1997), the two forces are in the same sense so that a steady flow cannot be reached. (Note that, in this northward flow case, the scale of the flow is the familiar midlatitude Rossby radius so that the β force is small and unimportant.)

3. Solution

A schematic diagram of the downstream solution is shown in Fig. 2b. As mentioned, in order for the balance given by (2.3) to hold, a broad flow field is established. This way the second term can become as large as the first one (even if the transport ψ is of order unity). In this scenario the jet on the left-hand side (looking downstream) is of the conventional midlatitude Rossby radius (R_d) but the sluggish interior is of the equatorial Rossby radius R_{de}. It is assumed here (and later verified with the numerics) that friction has brought the region into which the outflow does not penetrate quickly to rest.

The ratio between the two scales R_d/R_{de} is $O[(\beta R_d/f_0)^{1/2}]$, which is usually small, typically $\sim O(0.1)$. In view of this, the second term in (2.3) can be approximated by an integration over the sluggish interior. Namely, (2.3) can be approximated by

$$\int_{-L}^{0} hu^2\, dy = \beta \frac{g' H L^2}{4 f_0}. \tag{3.1}$$

In what follows, this equation will be used to construct the solution for both zero and finite potential vorticity flows.

a. Zero potential vorticity

In this case (i.e., $v_x - u_y + f = 0$), the speed within the jet is linearly distributed:

$$u = f(y - w + L), \tag{3.2}$$

where ($L - w$) is the interior width and $w = \sqrt{2}(g'H)^{1/2}/f_0$ (Fig. 3). This velocity reaches a maximum ($-fw$) near the outer edge ($y = -L$) and zero along the boundary between the jet and the sluggish interior ($y = -L + w$). Geostrophy shows that the thickness within the jet is parabolic:

$$h = -f_0^2(y + L)^2/2g' + f_0^2 w(y + L)/g', \tag{3.3}$$

where, again, $w = \sqrt{2}(g'H)^{1/2}/f_0$. This thickness vanishes along the outer edge ($y = -L$) and reaches the value H along the inner edge (i.e., $y = -L + w$).

Substitution of (3.2) and (3.3) into (3.1) ultimately leads to

$$L = \left(\frac{\sqrt{2}16}{15}\right)^{1/2} \frac{(g'H)^{1/4}}{\beta^{1/2}} = 1.228 R_{de}, \tag{3.4}$$

where, as before, $H = (2 f_0 Q/g')^{1/2}$ and R_{de} is the equatorial Rossby radius, $(g'H)^{1/4}/\beta^{1/2}$. This is our desired solution for the downstream outflow width.

b. Finite potential vorticity

We shall now consider two cases of finite potential vorticity flows. In the first case, the potential vorticity depth H_p is identical to the undisturbed depth H and in the second the two depths are not necessarily the same; that is, $H_p \neq H$.

1) $H_p = H$

In this case both velocity and thickness decay exponentially with y/R_d and the velocity has a maximum value of $(g'H)^{1/2}$ along the edge ($h = 0$). In a similar fashion to the zero potential vorticity calculation, one ultimately finds

$$L = \left(\frac{2}{3}\right)^{1/2} \frac{(g'H)^{1/4}}{\beta^{1/2}} = 0.816 R_{de}. \tag{3.5}$$

We see that the finite PV outflow is narrower than that of the zero PV outflow because the velocities and, hence, the jet force are smaller.

2) $H_p \neq H$

In this case the velocity and thickness profiles have both an exponential growth and an exponential decay. Although the solution is straightforward, its derivation is somewhat tedious. The jet's velocity and thickness profiles are

$$u = \left(\frac{A}{R_d}e^{-y/R_d} - \frac{\beta}{R_d}e^{y/R_d}\right)\frac{g'}{f_0} \quad \text{and} \tag{3.6}$$

$$h = Ae^{-y/R_d} + Be^{y/R_d} + H_p, \tag{3.7}$$

where $R_d = \sqrt{g'}H_p/f_0$, and A and B are constants that need to be determined. The thickness h vanishes at $y = -L$ and the velocity u vanishes at the edge of the stagnant region, $y = -L + w$ (where w is the width of the jet). Also, the thickness must match at the edge of the stagnant region ($y = -L + 2$); that is, $h = H$ there. These three conditions enable us to find the solution for the three unknowns A, B, and w. By defining $E = e^{w/R_d}$, the following three algebraic equations are obtained from the above conditions:

$$A = BE^2, \tag{3.8}$$

$$A + BE^2 + (H_p - H)E = 0, \quad \text{and} \tag{3.9}$$

$$A + B + H_p = 0. \tag{3.10}$$

Noting that E must be positive and that $E \to \infty$ in the limit $H_p \to H$, one finds after some algebra

$$E = \frac{-H_p - [H_p^2 - (H - H_p)^2]^{1/2}}{(H - H_p)}, \tag{3.11}$$

$$A = -E^2H_p/(1 + E^2), \quad \text{and} \tag{3.12}$$

$$B = -H_p/(1 + E^2), \tag{3.13}$$

which now enables us to solve the problem. Substitution of (3.12)–(3.13) into (3.1) gives [via Mathematica software (Wolfram 1996)] the desired expression for L:

$$L = \left[\frac{2}{3}\frac{(E^2 - 1)(1 + 10E^2 + E^4) - 12E^2(1 + E^2)\log(E)}{(1 + E^2)^3}\left(\frac{H_p}{H}\right)^{5/2}\right]^{1/2}\frac{(g'H)^{1/4}}{\beta^{1/2}}, \tag{3.14}$$

where E is given by (3.11). This solution (which is shown in Fig. 5) completes the derivation of the analytical solution, which as we shall see in the next section, compares favorably with the numerical simulations.

4. Numerical simulations

To further analyze the validity of our assumptions (e.g., that the flow is parallel to the wall downstream), we shall now present numerical simulations and quantitatively analyze the results.

a. Numerical model description

We used the Bleck and Boudra (1986) reduced-gravity isopycnic model with a passive lower layer and employed the Orlanski (1976) second-order radiation condition for the open boundary in the west. We found that this condition is satisfactory because the downstream streamlines were not significantly disturbed when they crossed the boundary. To speed up the experiments (which make our runs more economical) and reduce the effect of friction, we used a magnified value for β in most of our experiments. Specifically, we performed two kinds of experiments. The first kind were those with an intense zero potential vorticity outflow, whereas the second group were those with a finite potential vorticity. Within each group the results were very similar to each other and, consequently, we present here only one experiment of each group. As is typical for these kinds of experiments, our wall was slippery and we took the vorticity to be zero next to it.

For economical reasons, the runs were conducted with a (magnified) β of 10^{-10} m^{-1} s^{-1} that shortens the integration period because it increases the Rossby wave speed. We chose a relatively high resolution correspond-

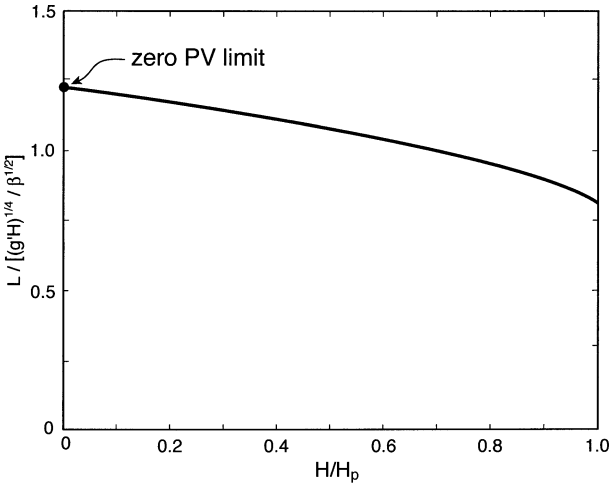

FIG. 5. The analytical solution for the general finite potential vorticity case: H_p is the potential vorticity depth and H is the thickness of the stagnant region [related to the transport by $H = (2f_0Q/g')^{1/2}$]. Note that $H/H_p \to 0$ is the zero PV limit [$L/R_{de} = (\sqrt{216}/15)^{1/2}$] and that $H/H_p \to 1$ is the finite PV limit for our special case, [$L/R_{de} = (2/3)^{1/2}$]. Also, note that despite the broad range of H/H_p, the difference between the zero PV and finite PV is not that large.

ing to $\Delta x = \Delta y = 5.4$ km. For numerical stability, we chose an eddy viscosity of 500 $m^2\ s^{-1}$; the time step was 5 min and the undisturbed thickness H was 470 m. These choices are certainly adequate for a Rossby radius of 30 km (corresponding to a g' of 2×10^{-2} m s^{-2} and $f_0 = 10^{-4}\ s^{-1}$). Furthermore, these choices always allowed for at least 10 grid points across the downstream current, which is also adequate. Our mass flux was always 22 Sv (Sv $\equiv 10^6\ m^3\ s^{-1}$) and we used a narrow feeding channel instead of a point source. We chose the channel width so that the upper-layer thickness was zero along the left wall (looking downstream); the thickness along the right wall was 470 m. We ran both the zero PV and the finite PV experiment for a long enough time (2300 days) so that the initial eddy (which will be shortly discussed) was removed.

b. Results

The results are shown in Figs. 6–9. All show reasonable agreement with the theory despite the fact that the error in the approximation is relatively large [$O(\beta R_d/f_0)^{1/2}$, which is roughly 0.2]. Initially, immediately after the light fluid starts pouring into the basin, the outflow is too small to sense β. Consequently, the solution is the Nof and Pichevin (2001) f-plane solution; that is, a growing eddy is established to the right of the source (looking downstream). After some time, however, the eddy becomes large enough to sense β and it is gradually forced westward. Ultimately, the influence of β is so large that the tendency of the eddy to drift westward exceeds its growth rate so that it detaches and drifts westward. Later on it is removed from the area altogether and, at that point, it completes its role in the establishment of the outflow.

Two additional points should be made about the eddy. First, stationary anticyclones next to a wall leak fluid on the left (looking onshore) but our eddy is moving so that the leak is ''swallowed'' by the migrating eddy. Second, lenses embedded in a lower layer of finite depth are unstable (e.g., Saunders 1973; Griffiths and Linden 1981) but they are stable in an infinitely deep lower layer (Paldor and Nof 1990), which is the case here.

Figures 6 and 7 show that, as the theory predicts, a long broad current is indeed established (after the initial eddy has moved downstream). The flow separates from the wall to the right of the source but this has no bearing on our solution, even in the limit of no viscosity (which may involve velocity discontinuities) because the equations that are used must still be satisfied. We see that the velocities in the nearly stagnant region are, indeed, very small in comparison with the speeds within the jet. Specifically, the thickness contours clearly show that the speeds there are no more than 10% of those within the jet.

In some sense, Fig. 8 is the ''backbone'' of our analytical–numerical comparison because it shows the momentum balance corresponding to (2.3). We see that, although the fluxes vary with time, at each moment the integrated forces balance each other. Namely, Fig. 8 illustrates that there are no unaccounted forces and that, despite the fact that frictional effects may accumulate over time to become an important effect (in some sense), at each moment in time the inviscid balance of forces is an excellent approximation to the problem. Figure 9 shows a comparison of the analytical and numerical widths of the zero and finite PV outflows. The error is less than 15%, which is well within the error of the calculation resulting from the neglect of the jet's width in comparison with the width of the nearly stagnant region [as mentioned earlier, it is $\sim O(\beta R_d/f_0)^{1/2}$, which is roughly 0.2]. Aside from this neglect, there are two additional differences between the numerics and the analytics. One is associated with the assumption that, because of frictional effects, the region into which the jet does not penetrate is motionless. In reality, the speeds there are small, about a tenth of the speed in the jet (see Figs. 6 and 7), but they are not entirely negligible. The second difference results from frictional effects that cause lateral spreading of both the jet and the nearly stagnant region.

Since the speeds in the zero PV case are greater than those of the finite PV case, friction is more important in the former and, as expected, the discrepancy between the numerics and the analytics is greater. To verify that friction can indeed bring the region near the wall to rest, even when the PV has to change significantly, we also conducted a numerical simulation with incoming cyclonic rather than anticyclonic vorticity. We took the incoming shear to be $f/2$, the width w to be 43 km, H to be 470 m, and the discharge to be again 22 Sv. In this case, the PV was obviously not uniform and corresponded to the region outside the range shown in Fig. 9. The results were very similar to our other experiments. This is not very surprising given the fairly weak dependence of the solution on the PV (Fig. 9).

c. Limitations

As is usually the case, the analytical and numerical models both have their limitations. The two most important weaknesses of the analytical solution result from the fact that we did not find the complete first-order solution and the use of a 1½-layer model. (Note that the latter limitation is also present in the numerics.) We shall take these two issues one by one. The first limitation can be important because the complete first-order solution (i.e., the solution for both upstream and downstream fields) may impose constraints that may restrict the validity of our solution. Our second limitation (resulting from the 1½-layer approach) excludes baroclinic instabilities (of both the initial eddy and the downstream current) and prevents the radiation of energy outward. This essentially eliminates a nonfrictional decay from the problem.

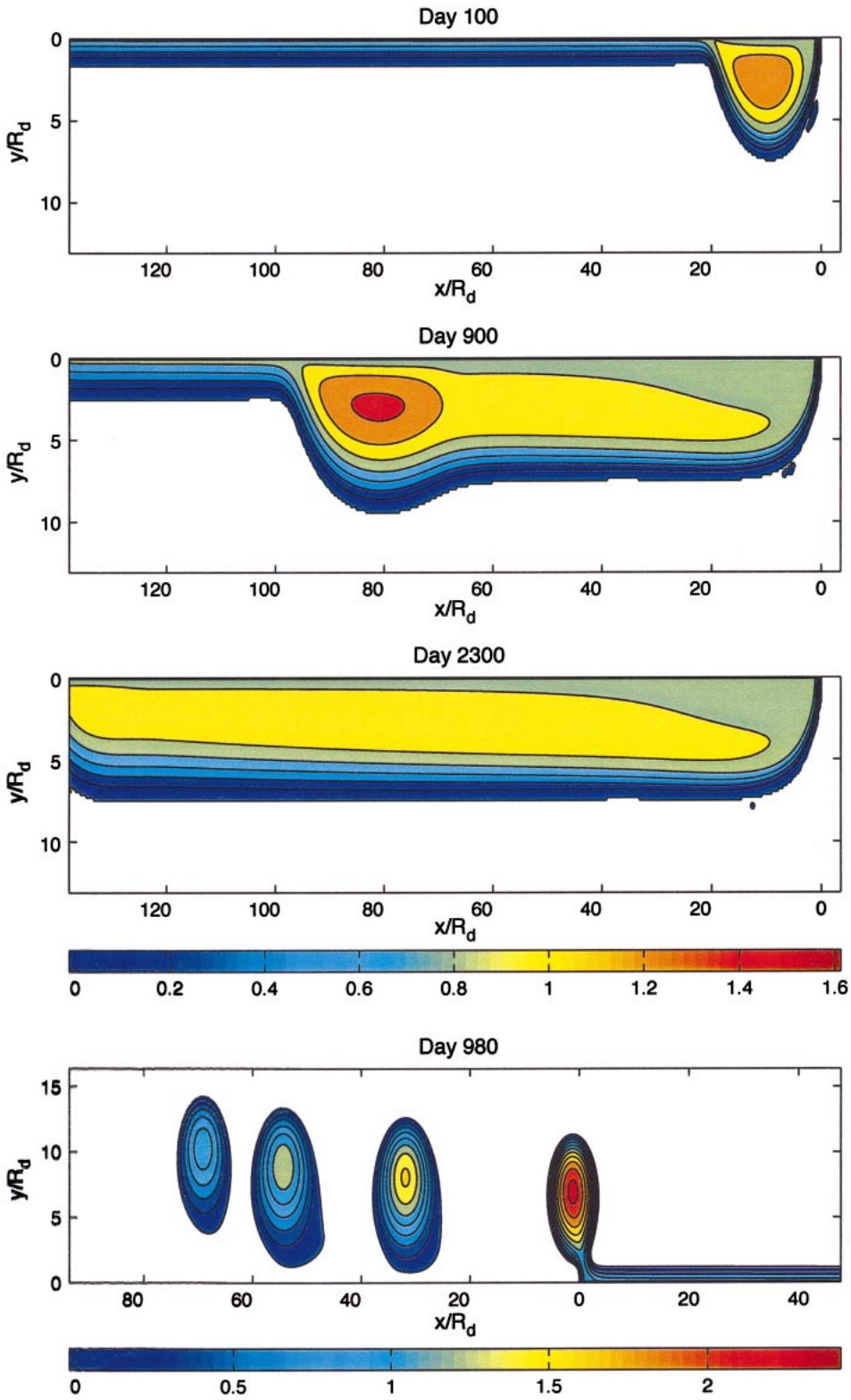

FIG. 6. (Top three panels) Nondimensional thickness contours for a southward outflow with zero potential vorticity. We see that, after an initial eddy is produced (á là Nof and Pichevin 2001), a steady broad current is established. The gradient of the thickness contours clearly shows that most of the outflow is nearly stagnant but that a swift jet is present away from the wall. Specifically, the gradients (and, hence, the speeds) in the nearly stagnant regions are about 1/10 of what they are within the jet. (bottom) For a comparison, a northward eddy-producing outflow (Pichevin and Nof 1997) is also shown. Note that the meridional scale is stretched to show the structure of the southward outflow more clearly. As a result, the bottom-panel eddies appear to be very elongated.

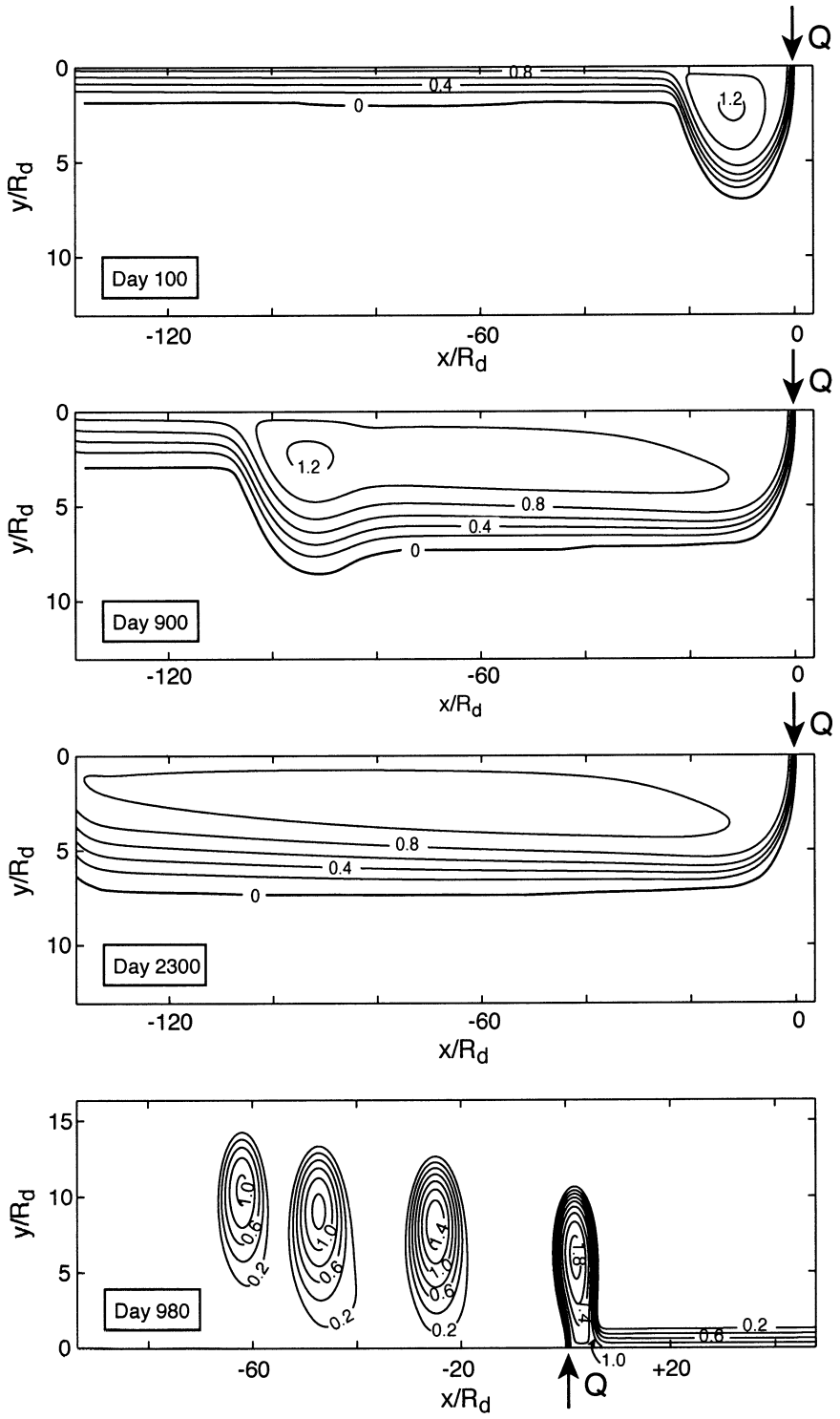

FIG. 7. Same as the zero potential vorticity case (Fig. 6) except that the outflow's potential vorticity is now finite (H_p = 1100 m; H = 470 m). It shows that the difference between the two is minimal.

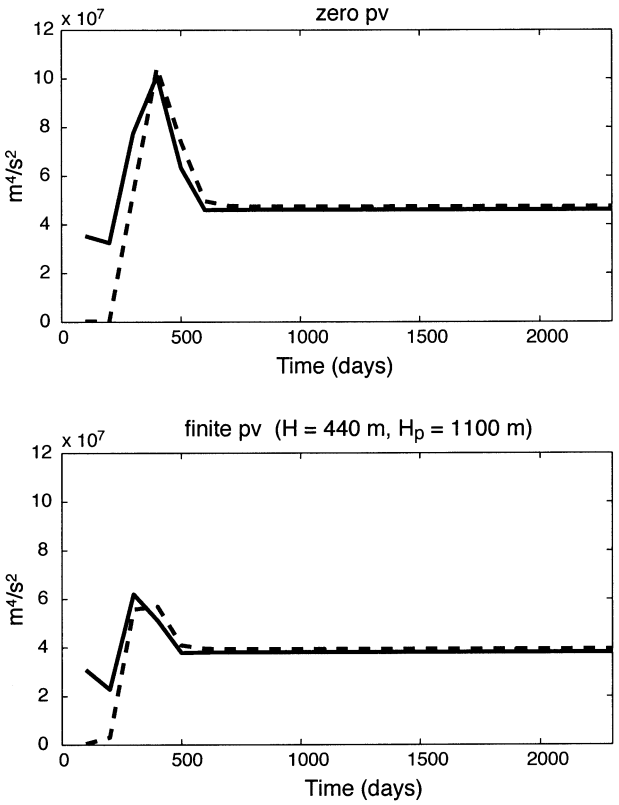

FIG. 8. The numerical jet force (solid line) and the β force (dashed line) corresponding to (2.3). The two terms are almost identical, indicating that (2.3) is a valid approximation to the balance. The numerical measurements were made at $x/R_d = -32$. The apparent steadiness of the momentum flux is due to the integration, which smooths variations. The details of the flow are not that steady (Figs. 6 and 7).

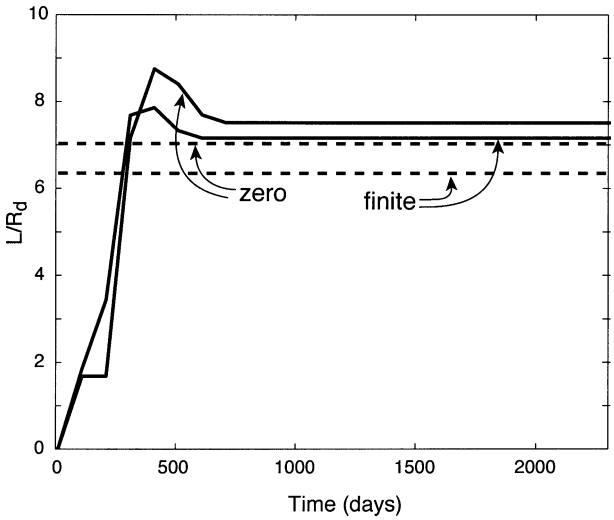

FIG. 9. The analytical (dashed lines) and numerical (solid lines) widths (at $x/R_d = -32$) for the zero and finite potential vorticity experiments. The difference between the analytics and the numerics is less than 15%, indicating that our approximations are valid. This difference is primarily because of three flow properties. The first is that the neglected terms in the analytics are of $O(\beta R_d/f)^{1/2}$, which is approximately 0.18. The second is that what is assumed to be stagnant in the analytics is not exactly stagnant in the numerics, and the third is that friction tends to spread the flow.

5. Summary and discussion

We have considered here the last unsolved case of a nonlinear, inviscid outflow debouching into a square basin on a β plane. It is the case of a southward outflow (Fig. 1). It turns out that this outflow behaves very differently from the other three that were considered earlier [northward (Pichevin and Nof 1997), eastward (Nof and Pichevin 1999), and westward (Nof et al. 2002)] because it is the only one that does not involve a stationary eddy or periodically generated eddies (Fig. 1). It is for this reason (and our misconception that it should involve eddies) that it was the most difficult solution for us to obtain even though it is by far the simplest solution of the four.

The results of our theory can be summarized as follows:

1) The nonlinear inviscid southern outflow involves a very broad westward flow consisting of a nearly stagnant region near the wall and a jet on the ocean side (see Fig. 2b and the numerical results shown in the upper three panels of Figs. 6 and 7). The nearly stagnant region width is on the order of the equatorial Rossby radius, $R_{de} \equiv (g'H)^{1/4}/\beta^{1/2}$. [It is $1.228R_{de}$ for a zero PV outflow and $0.816\ R_{de}$ for a uniform PV whose potential vorticity depth matches the undisturbed depth. It is given by (3.14) for the most general case of a uniform PV whose potential vorticity depth does not necessarily match the undisturbed depth.] The jet's width is the familiar midlatitude Rossby radius R_d.
2) The general analytical solution (3.4), (3.5), and (3.14) corresponds to a balance between two alongshore forces, the rocketlike ''jet'' force resulting from the dynamic momentum flux of the intense narrow flow near the edge and the westward β-induced force associated with the nearly stagnant region (2.3). Such a balance does not hold in the *northward* outflow case (examined by Pichevin and Nof 1997) because, in that case, the jet and β forces are pointing in the same direction. As a result, an entirely different, time-dependent balance takes place and eddies are generated on the west side (Figs. 6 and 7, lower panels).
3) The above results are in very good agreement with the numerics (Figs. 8 and 9). The main difference between the analytical and the numerical simulations is the neglect of the jet's width and friction in the analytics.
4) Friction enters the problem in two ways. First, it brings the region into which the steady outflow does not penetrate (i.e., the broad region next to the wall) to rest by changing its potential vorticity. Second, it spreads the jet, causing it to broaden downstream.

The above calculation should have numerous appli-

cations (e.g., the surface waters flowing from the Atlantic to the Caribbean via the Windward and Mona Passages), but it is one of these rare cases in which the theory is ahead of the observations simply because there are presently no measurements to support or refute it. Although measurements in and around those passages have been made (e.g., Johns et al. 1998), it is not presently possible to say what the downstream width is. One would hope that general numerical simulations would help to bridge this gap, but such models do not usually resolve the passage dynamics so that they cannot be used for this purpose. It is hoped that this study will encourage future observational programs to look at the outflow length-scale issue.

It is important to realize that, even if the observations of the relevant outflows were easy to conduct, it is still not clear that they can be easily compared to the theory. The theory ignores the effects of winds, tides, and friction, and all of these can, no doubt, alter the results dramatically, particularly if the outflow does not carry a significant amount of anomalous water. Although this is definitely a limitation of our study, it should be kept in mind that the three complementary cases shown in Fig. 1 (northward outflow, eastward outflow, westward outflow) do show good agreement with observations, indicating that the effects of winds, tides, and friction can be, at least in some cases, marginal. Last, it will be useful to extend the theory to the cases in which the walls are slanted so that a combination of the four cases shown in Fig. 1 will be active. Namely, it will be useful to extend the square basin (shown in Fig. 1) to a basin with the shape of a hexagon.

Acknowledgments. Two reviewers provided useful comments on the manuscript. This study was supported by National Aeronautics and Space Administration Grant NAG5-10860, National Science Foundation Contracts OCE 9911324 and 0241036, and Office of Naval Research Grant N00014-01-0291.

APPENDIX

List of Variables

f	Coriolis parameter
f_0	Coriolis parameter at the origin
F_B	Planetary gradient force
g'	Reduced gravity
h	Thickness
H	Undisturbed depth
H_p	Potential vorticity depth
L	Length scale in the y direction
Q	Incoming mass flux
R_d	Rossby radius
R_{de}	Equatorial Rossby radius
S	Integration area
u, υ	Velocity in the x and y directions
u_s	Speed at the source
U, V	Velocity scales in the x and y directions
w	Width
β	Variation of the Coriolis parameter with latitude
ϕ	Boundary of the integration area
ρ	Density
ψ	Streamfunction (defined by $\partial\psi/\partial y = -uh$; $\partial\psi/\partial x = -\upsilon h$)

REFERENCES

Bleck, R., and D. Boudra, 1986: Wind-driven spin-up in eddy-resolving ocean models formulated in isopycnic and isobaric coordinates. *J. Geophys. Res.,* **91,** 7611–7621.

Bormans, M., and C. Garrett, 1989: A simple criterion for gyre formation by the surface outflow from a strait, with application to the Alboran Sea. *J. Geophys. Res.,* **94,** 12 637–12 644.

Chao, S.-Y., and B. Boicourt, 1986: Onset of estuarine plumes. *J. Phys. Oceanogr.,* **16,** 2137–2149.

Defant, A., 1961: *Physical Oceanography.* Vol. I, Pergamon Press, 729 pp.

Fong, D. A., 1998: Dynamics of freshwater plumes: Observations and numerical modeling of the wind-forced response and alongshore freshwater transport. Ph.D. thesis, Woods Hole Oceanographic Institution/Massachusetts Institute of Technology, 172 pp.

Garvine, R. W., 1987: Estuary plumes and fronts in shelf waters: A layer model. *J. Phys. Oceanogr.,* **17,** 1877–1896.

——, 1996: Buoyant discharge on the inner continental shelf: A frontal model. *J. Mar. Res.,* **54,** 1–33.

——, 2001: The impact of model configuration in studies of buoyant coastal discharge. *J. Mar. Res.,* **59,** 193–225.

Griffiths, R. W., and P. F. Linden, 1981: The stability of vortices in a rotating, stratified fluid. *J. Fluid Mech.,* **105,** 283–316.

Horner, A. R., D. A. Fong, J. R. Koseff, T. Maxworthy, and S. G. Monismith, 2000: The control of coastal current transport. *Proc. Fifth Int. Symp. on Stratified Flow,* Vancouver, BC, Canada, International Association of Hydraulic Research, 865–870.

Johns, W. E., T. N. Lee, R. C. Beardsley, J. Candela, R. Limeburner, and B. Castro, 1998: Annual cycle and variability of the North Brazil Current. *J. Phys. Oceanogr.,* **28,** 103–128.

Kourafalou, V. K., L.-Y. Oey, J. D. Wang, and T. N. Lee, 1996: The fate of river discharge on the continental shelf. 1. Modeling the river plume and the inner shelf coastal current. *J. Geophys. Res.,* **101,** 3415–3434.

Nof, D., 1978a: On geostrophic adjustment in sea straits and wide estuaries: Theory and laboratory experiments. Part I: One-layer system. *J. Phys. Oceanogr.,* **8,** 690–702.

——, 1978b: On geostrophic adjustment in sea straits and wide estuaries: Theory and laboratory experiments. Part II: Two-layer system. *J. Phys. Oceanogr.,* **8,** 861–872.

——, 1988: Outflows dynamics. *Geophys. Astrophys. Fluid Dyn.,* **40,** 165–193.

——, and T. Pichevin, 1999: The establishment of the Tsugaru and the Alboran gyres. *J. Phys. Oceanogr.,* **29,** 39–54.

——, and ——, 2001: The ballooning of outflows. *J. Phys. Oceanogr.,* **31,** 3045–3058.

——, J. Sprintall, and T. Pichevin, 2002: ''Teddies'' and the origin of the Leeuwin Current. *J. Phys. Oceanogr.,* **32,** 2571–2588.

O'Donnell, J., 1990: The formation and fate of a river plume: A numerical model. *J. Phys. Oceanogr.,* **20,** 551–569.

Oey, L.-Y., and G. L. Mellor, 1993: Subtidal variability of estuarine outflow, plume, and coastal current: A model study. *J. Phys. Oceanogr.,* **23,** 164–171.

Orlanski, I., 1976: A simple boundary condition for unbounded hyperbolic flows. *J. Comput. Phys.*, **21,** 251–269.
Paldor, N., and D. Nof, 1990: Linear instability of an anticyclonic vortex in a finite depth ocean. *J. Geophys. Res.*, **95,** 18 075–18 080.
Pichevin, T., and D. Nof, 1997: The momentum imbalance paradox. *Tellus*, **49,** 298–319.
Rhines, P. B., 1975: Waves and turbulence on a beta-plane. *J. Fluid Mech.*, **69,** 417–443.
Saunders, P. M., 1973: The instability of a baroclinic vortex. *J. Phys. Oceanogr.*, **3,** 61–65.
Takano, K., 1954: On the velocity distribution off the mouth of a river. *J. Oceanogr. Soc. Japan*, **10,** 60–64.
——, 1955: A complementary note on the diffusion of the seaward river flowing off the mouth. *J. Oceanogr. Soc. Japan*, **11,** 147–149.
Whitehead, J. A., 1985: The deflection of a baroclinic jet by a wall in a rotating fluid. *J. Fluid Mech.*, **157,** 79–93.
——, and A. R. Miller, 1979: Laboratory simulation of the gyre in the Alboran Sea. *J. Geophys. Res.*, **84,** 3733–3742.
Wolfram, S., 1996: *The Mathematica Book.* Addison-Wesley, 1395 pp.
Yankovsky, A. E., and D. C. Chapman, 1997: A simple theory for the fate of buoyant coastal discharges. *J. Phys. Oceanogr.*, **27,** 1386–1401.